Journal of Materials Chemistry A

Accepted Manuscript

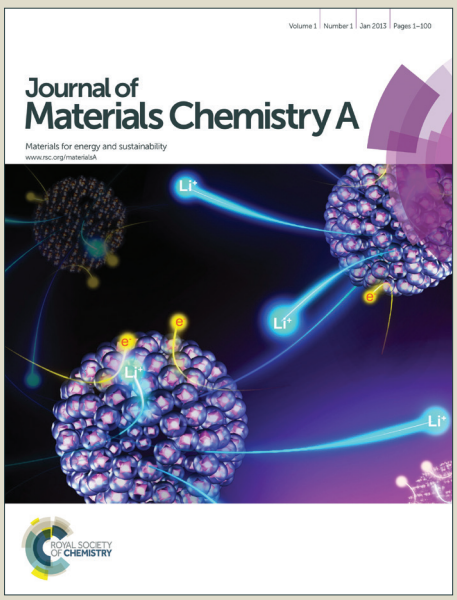

ROYAL SOCIETY OF CHEMISTRY

www.rsc.org/materialsA

Journal Name

RSCPublishing

ARTICLE

Plasmonic enhanced self-cleaning activity on asymmetric Ag/ZnO SERS substrates under ultraviolet and visible irradiation†

Cite this: DOI: 10.1039/x0xx00000x

Received 00th January 2012,
Accepted 00th January 2012

DOI: 10.1039/x0xx00000x

www.rsc.org/

Yashu Zang,[a] Jun Yin,[a,b] Xu He,[a] Chuang Yue,[a] Zhiming Wu,[a] Jing Li,*[a] and Junyong Kang*[a]

Two different asymmetric Ag/ZnO composite nanoarrays are fabricated and proposed to be used as highly sensitive and uniform surface-enhanced Raman scattering (SERS) substrates with plasmonic enhanced ultraviolet (UV)-visible photocatalytic property for self-cleaning. These two asymmetric nanostructures are composed of Ag nanoparticles (NPs) hanging inside or capping on the top of ZnO hollow nanospheres (HNSs), which allow the generation of strong local electric-field near the contact area owing to the asymmetric dielectric environment. Experimental and simulation results reveal that these asymmetric structures are much favorable for achieving high photocatalytic activity under UV and visible light irradiation besides improving the SERS performance. The electron transfer model based on the band-gap alignment was employed to further illustrate the mechanisms of the irradiation wavelength dependent photocatalytic activity. Given the dramatically improved photocatalytic performance together with the reproducible and uniform SERS signals verified by the Raman mapping results, the large area ordered asymmetric metal/semiconductor nanoarrays have been demonstrated to be suitable for the further applications in multifunctional photoelectrochemical chips.

1. Introduction

Surface-enhanced Raman scattering (SERS) technique has been widely investigated as a powerful tool for ultra-sensitive vibrational spectroscopy leading to wide applications in analytical chemistry, medicine, and life science, *etc*.[1-5] The local electromagnetic field enhancement induced by the surface plasmon resonance (SPR) from the noble metal nanostructures is well accepted as the major mechanism for SERS.[6] Generally, designing various metal nanostructures, with roughened surfaces or in the form of nanoparticles (NPs), were often emphasized with the concern for Raman scattering enhancements.[2,7] However, from the viewpoint of practical detections, preparing structures embracing both SERS and self-cleaning functions as recyclable sensing chips is more meaningful.[8-10] Up to date, a number of approaches have been extended to fabricate multi-functional SERS-photocatalytic substrates by compositing noble metals with semiconductor materials, such as Ag or Au/TiO_2,[8,9] Au/ZnO[10] and so on. Recently, TiO_2 have been studied by many researchers concentrating on improving its photocatalytic activity for photo-degradation of organic pollutions or water splitting.[11-13] ZnO, as a direct wide band gap (WBG) semiconductor with a similar large excitation binding energy as that in TiO_2, also shows good performances in photocatalytic reactions besides its well-known applications in dye-sensitized solar cells (DSSC), or organic solar cells.[14-16] Previous studies have demonstrated that ZnO presents more efficiency than TiO_2 in photocatalytic degradations of reactive blue 19, 2-phenylphenol, and rhodamine 6 G (R6G).[17-19] Moreover, the feasibility of synthesizing different ZnO morphologies with high surface volume ratio, such as nanowires,[20] nanoflowers,[21] nanotetrapods,[22] *etc*., also makes it an ideal candidate as photocatalyst. Unfortunately, the fundamental drawback to ZnO is that it hardly utilizes the main parts of the solar energy in the visible region because of its WBG of about 3.3 eV, generally resulting in unsatisfied conversion efficiencies.[23] While, it is well acknowledged that besides the SERS function the geometrical configuration of metal/semiconductor composites can also significantly improve the photocatalytic efficiency by (i) increasing light absorption in semiconductor when the plasmon resonance energies overlapping with band gap absorption of the semiconductor, (ii) reducing the electron/hole diffusion length in nanostructures, and (iii) forcing the electron-hole separation by transferring the energetic electrons between metal and semiconductor.[24-27] Therefore, designing and fabricating metal/semiconductor composites in different morphologies and contact forms, like core/shell[8,28] or janus

nanostructure[13] *etc*., could be a fundamentally feasible strategy to accomplish both high SERS sensitivities and enhanced photocatalytic efficiencies on a multi-functional SERS substrate.

In this work, two asymmetric directly contact metal/semiconductor (Ag/ZnO) hybrid nanoarrays in different configurations and contacts were fabricated by the nanosphere lithography (NSL) technique,[29-31] and used as SERS-active substrates with the self-cleaning functionalities in both UV and visible light irradiation. Besides high sensitive SERS phenomena, reproducible plasmonic assisted self-cleaning properties are realized in these highly sensitive asymmetric Ag/ZnO nanoarray SERS substrates, which are suggested to be caused by the extremely strong local field enhancement near the contact areas of metal/semiconductor. The experimental extinction spectra and simulated near-field distributions in these hybrid nanoarrys further evidence the enhanced SPR properties. Moreover, the electron transfer model combined with the band-gap alignment was proposed to explain the distinguishable photocatalytic mechanisms in these geometrically different asymmetric Ag/ZnO nanocomposits under UV and visible light irradiation, respectively. Given the simple and Si-compatible fabrication process, these kind of multi-functional asymmetric metal/semiconductor nanocomposite substrates are fundamentally and technically applicable in practical integrated recyclable sensing chips.

2. Experimental Section

2.1 Fabrication of the asymmetric nanostructure arrays

Experimentally, the two different composite nanostructures of Ag NPs hanging inside and capping on ZnO hollow nanospheres (HNSs) were fabricated using the polystyrene (PS) nanospheres as template followed by the radio-frequency (RF) magnetron sputtering deposition and a thermal treatment. The fabrication process of the Ag NPs on the top of ZnO HNSs (simplified as AOZ) can be referred to our previous procedures,[32] while the Ag NPs inside ZnO HNSs (simplified as AIZ) were prepared by reversing the film depositing orders of Ag and ZnO. In brief, the monolayer PS nanospheres (7 wt%) with the diameter of ~360 nm were firstly self-assembled on wet-chemically cleaned Si substrates using spin-coating method. In order to obtain the suitable size and distribution of the periodic nanoarrays, the PS template can be manipulated by O_2 plasma etching. Then the Ag and ZnO films with both thicknesses of 20 nm were successively deposited in the sequence of ZnO and Ag or Ag and ZnO on the PS templates at the room temperature employing RF magnetron sputtering followed by a thermal treatment at 500 °C for 30 minutes in N_2 ambient. Consequently, two kinds of asymmetric hybrid nanostructures were produced with Ag NPs capping on or hanging inside the top surfaces of ZnO HNSs.

2.2 Characterization

The morphologies and structure properties of the composites were investigated using a field emission scanning electron microscopy (SEM, Hitachi S-4800). A UV-visible spectrophotometer (Varian Cary 300) was employed to collect the extinction spectra of all the samples. The SERS characterization of asymmetric Ag/ZnO nanoarrays was performed on Renishaw inVia Raman Microscope using the 532-nm laser excitation source and analyte of R6G. The photocatalytic activities of those two samples under UV and visible light irradiation were evaluated by the Raman signals' intensity of R6G on corresponding substrates. During the photocatalytic processes, a 18 W Philips UV lamp emitting line ranging from 340 to 410 nm with a main wavelength at 365 nm and an Xenon lamp (500 W) with a UV light filter (cut-off at the wavelength of 400 nm) in an optical power of 100 mW cm^{-2} were used as the UV and visible light sources, respectively. The Raman mapping was then carried out on a confocal Raman imaging system (WITec Confocal Raman Microscope Alpha 300) equipped with a 488 nm laser excitation source.

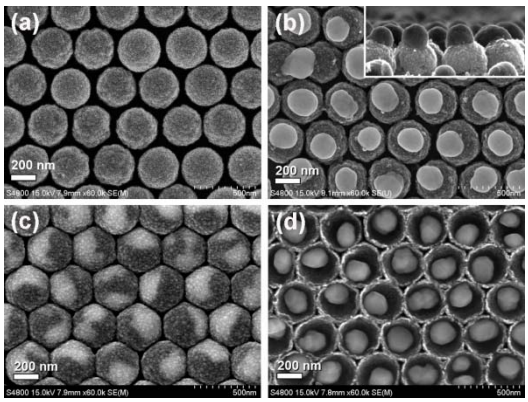

Fig. 1 SEM images of the (a) ZnO HNS arrays, (b) AOZ arrays, and (c) top and (d) inside morphologies of AIZ arrays. To obtain the inside information of the AIZ structure, the arrays on silicon substrate were lifted off by conductive tape and then the inverted AIZ structure was characterized.

3. Results and Discussion

3.1 As-fabricated asymmetric structures

Fig. 1 shows the SEM images of the hexagonally close-packed ZnO HNSs and two different asymmetric hybrid structures produced using the self-assembled PS nanospheres in the size of 360 nm as templates. The size and separation of PS spheres were adjusted employing the O_2 plasma etching for 15 s on the template so that the as-produced ZnO HNSs show the average diameter of 330 nm in periodic arrays, as seen in Fig. 1a. The subsequent Ag film deposition and thermal treatment help to aggregate the Ag NPs in ellipsoid shape with the axis sizes about 190, 190, and 150 nm directly capping on ZnO HNSs, denoted as AOZ sample, as shown in Fig. 1b and its inset. On the other hand, as displayed in Fig. 1c and d, the periodic ZnO HNS arrays with Ag NPs hanging inside, named as AIZ sample, were fabricated by reversing the deposition sequence of Ag and ZnO films, in which the similar sizes of ZnO HNSs and Ag NPs can be visualized. It should be noticed that during the fabrication processes the ZnO layer takes an important role

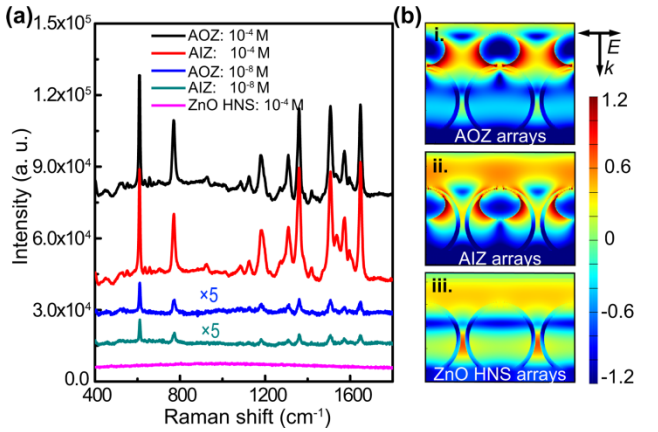

Fig. 2 (a) Raman spectra of R6G probe at the concentrations of 10^{-4} and 10^{-8} M on AOZ and AIZ arrays compared with that on the bare ZnO HNS sample at 10^{-4} M; (b) Simulated near-field distributions of (i) AOZ, (ii) AIZ, and (iii) bare ZnO HNS arrays on Si substrates under 532 nm light illumination (same with the laser source energy in the Raman measurements) with the intensity in log scale. The corresponding light incident and polarization directions are shown in the figure. The diameter and shell thickness of ZnO HNS were set as 330 and 20 nm, and the axis sizes of ellipsoid Ag NP in both nanocomposites are 190, 190, and 150 nm, which are consistent with the experimental parameters.

acting as a supporting template to form the two asymmetric structures and also exhibits different asymmetric dielectric environment.

3.2 SERS-active characterizations

A confocal Raman microscope with a 532-nm laser source was used to measure the SERS spectra of R6G on both asymmetric Ag/ZnO nanocomposites, which exhibit intensive Raman signals as shown in Fig. 2a. The resolved Raman vibration features of R6G, located at around 611, 771, 1361, 1418, 1574, and 1648 cm^{-1}, well agree with the reported data in the literature.[33] When reducing the concentration of R6G probe down to 10^{-8} M, distinguished Raman signals still can be identified in the Raman spectra on these two asymmetric nanostructures indicating their high SERS activities. Understandably, no Raman signal could be detected on the bare ZnO HNS arrays even with the R6G concentration of as high as 10^{-4} M due to the lack of SPR effect with the absence of metal decoration. Notably, the Raman signal intensity on the AIZ substrate is comparable to that on the SERS substrate of AOZ despite there is a 20-nm ZnO isolated layer.[34]

To further understand the SERS performances on these asymmetric structures, the near-field distributions of AOZ, AIZ, and bare ZnO HNS nanostructures under 532 nm light irradiation were simulated by finite difference time domain (FDTD) method as displayed in Fig. 2b. Compared with the bare ZnO HNSs, strong local field can be visualized around the Ag NPs in both asymmetric Ag/ZnO composite structures. Specifically, there is a much stronger field enhancement occurred at the contact region between the Ag NPs and ZnO HNSs in both structures, which is known as hot spots arising from the asymmetric dielectric environment around metal NPs and having been widely used for SERS.[13] Exceptionally, on the AIZ hybrid, besides a strong localized field in the contact area a considerable local field enhancement can still penetrate to the outer surface of ZnO layer, which is believed to be responsible for the Raman signal enhancement. Thus, both AOZ and AIZ are effective SERS active structures.

3.3 SPR property on the asymmetric structures

Fig. 3a shows the extinction spectra of the as-prepared AOZ and AIZ nanocomposites on sapphire substrate with comparison to the bare ZnO HNS arrays. In bare ZnO HNS substrate, besides the absorption edge at ~375 nm generally attributed to the near band-edge absorption of ZnO, another main extinction peak located at ~424 nm is resolved, which is believed to be originated from the whispering gallery mode (WGM) resonances of the ZnO hollow nanocavity arrays.[35] After decorating the Ag NPs either on or inside ZnO shell surface, an obvious extinction enhancement around 375 nm is observed and suggested to be due to the higher order SPR modes from the Ag NPs in a big size (the diameter larger than 100 nm).[36] Furthermore, a broad LSPR band covering the visible region ranging from 552 to 670 nm in AOZ arrays and centering at 533 nm in AIZ arrays can be distinguished. Undoubtedly, the different extinction features on the two kinds of Ag/ZnO asymmetric structures should be attributed to the size, shape and dielectric environment effects of metal NPs, which would be possible to affect the plasmonic assisted photocatalytic activity on the two structures in visible region.

Considering the possibility for enhancing photocatalytic performances by the LSPR effect in these asymmetric structures, the near-field distributions in these two hybrids were simulated employing both UV and visible light irradiation at the typical incident angles of 90° as shown in Fig. 3b and 45°

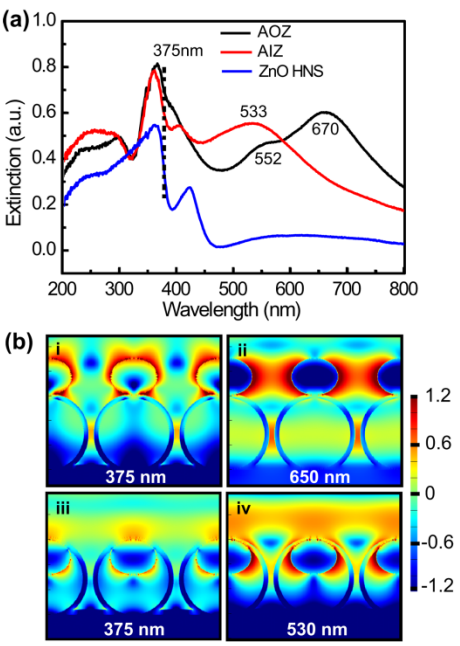

Fig. 3 (a) UV-visible extinction spectra of Ag NP on ZnO HNS (AOZ), Ag NP in ZnO HNS (AIZ) and ZnO HNS arrays on sapphire; (b) Simulated near-field distributions of the (i) and (ii) AOZ, and (iii) and (iv) AIZ nanostructures on the Si substrates under visible and UV light illumination, respectively. The intensity is in log scale.

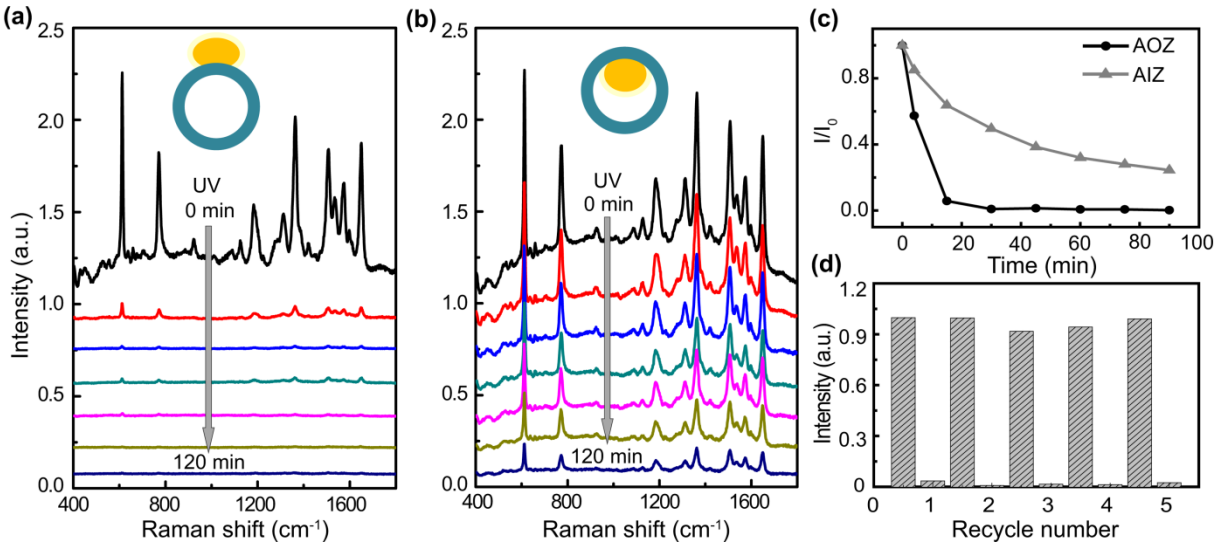

Fig. 4 SERS spectra of R6G (10^{-4} M) treated with UV light irradiation on the hybrid structures of the (a) AOZ and (b) AIZ arrays; (c) Self-cleaning activities on the two hybrids for degradation of R6G under UV light irradiation (Raman signal intensity radio $\eta = I/I_0$); (d) Reversible SERS behavior of R6G (10^{-4} M) on the AOZ substrate during repeated measurement-UV irradiation cycles.

illustrated in Fig. S1 of supporting information (SI). Under UV light illumination at the wavelength of 375 nm, matching with the band gap energy of ZnO, a strong local-field is presented near the interface of Ag/ZnO besides the high order SPR mode induced field around the Ag NPs in both samples as seen in Fig. 3b (i and iii), which is favorable for improving the photocatalytic properties by enhancing the light absorption in ZnO.[13] It should be noticed that the local near-field in AIZ hybrid is slightly weaker than that in AOZ structure possibly due to the more intrinsic absorption of ZnO near the band edge in this dielectric shell isolated structure. While, in the visible region, both the asymmetric structures can be found to show a highly enhanced dipole mode related local electrical field around Ag NPs as displayed in Fig. 3b (ii and iv), which might be potentially applied for enhancing the plasmonic assisted photocatalytic self-cleaning functionality within visible region.

3.4 Plasmonic assisted self-cleaning property

The plasmonic assisted self-cleaning process was firstly performed under UV light irradiation on the two asymmetric Ag/ZnO hybrid nanostructures and evaluated by the Raman signals' intensities afterwards. Fig. 4a and b show the SERS spectra of R6G adsorbed on these two substrates as a function of the UV-light irradiation time from 0 min to 120 min. It can be seen that the Raman signals' intensities of R6G probe on the geometrically different asymmetric structures both decline as

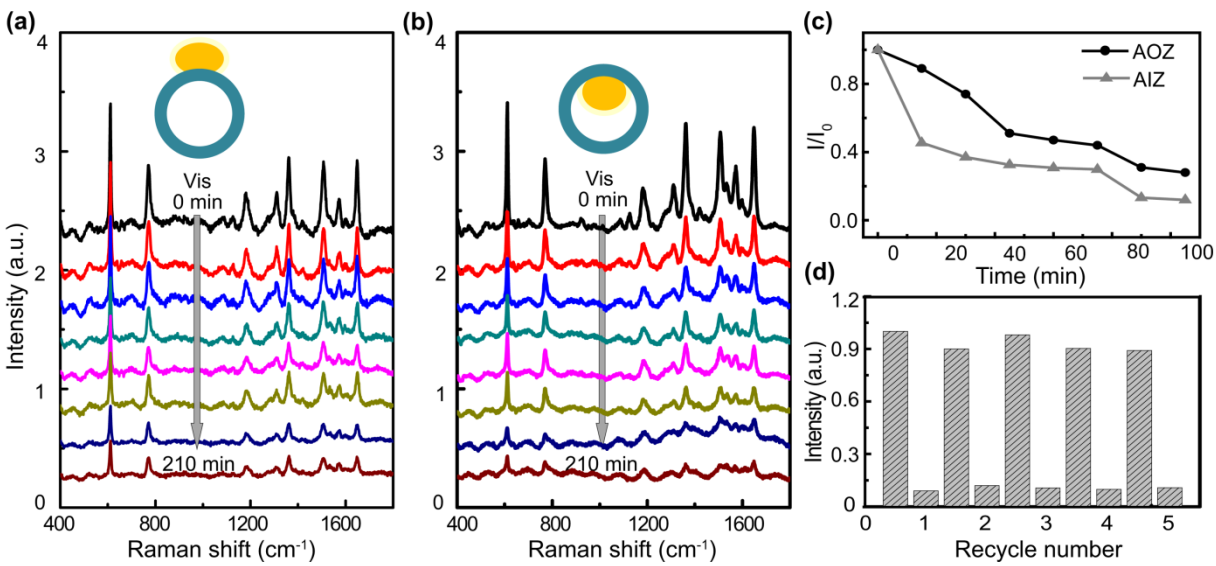

Fig. 5 SERS spectra of R6G (10^{-4} M) treated with visible light irradiation on the (a) AOZ and (b) AIZ arrays; (c) Self-cleaning activities on the two hybrids for degradation of R6G under visible light irradiation; (d) Reversible SERS behaviours of R6G (10^{-4} M) on AOZ during repeated measurement-visible irradiation cycles.

irradiation time increasing with the AOZ hybrid showing the quicker reduction, while there is no apparent changes on the bare ZnO HNS sample as shown in Fig. S2 (SI). The self-cleaning activities on these two samples were further compared by plotting the degradation rate of Raman signal $\eta = I/I_0$ (where η represents degradation ratio, and I_0 and I stand for the relative Raman signal intensity at about 611 cm^{-1} without and with UV or visible light irradiation for certain time), as shown in Fig. 4c. This statistically evidences the obvious photocatalysis mediated self-cleaning process in both nanostructures, although a significant higher photocatalytic activity is accomplished in the AOZ structure. The self-cleaning property of the AOZ structure was also verified by the repeated Raman measurement with R6G dropping and UV irradiation cycles as shown in Fig. 4d. As a result, the good recyclability still can be maintained on the as-prepared nanocomposite after five cycles of reuse processes.

Meanwhile, the self-cleaning activity on both AOZ and AIZ SERS substrates under visible light irradiation was also investigated as shown in Fig. 5. In spite of the absence of photo-generated carriers in this WBG semiconductor facilitating the photocatalytic process, an effective photo-degradation of R6G still can be realized on both of the asymmetric structures as seen in Fig. 5a and b. In this circumstance, hot electrons generated from the plasmonic effect are suggested to be the main reason for photocatalytic degradation of R6G agent.[27,37] However, the statistical degradation rate shown in Fig. 5c for the sample of AIZ seems slight faster than that of AOZ sample and this will be explained in the later part. The further performed recyclable examination on the AOZ composite confirms it to be an acceptable plasmonic assisted self-cleaning substrate with the good recyclability in the visible light irradiation, as shown in Fig. 5d.

3.5 Photocatalytic mechanisms

To better elucidate the reaction mechanisms in those asymmetric metal/semiconductor nanostructures under UV and visible light irradiation, the electron transfer model combined with the band-gap alignment was proposed as shown in Fig. 6. As the work function is different for ZnO (5.2 eV with the electron affinity of 4.5 eV) and Ag (4.2 eV), the Ohmic contact type of Ag/ZnO interface can be formed after the Fermi level equilibration, as shown in Fig. 6a (i) and b (i).[38,39] Under UV light irradiation, the possible reaction processes on the asymmetric Ag/ZnO samples are proposed as the following:[40,41]

$$ZnO + h\nu \rightarrow ZnO(e_{cb}^{-} + h_{vb}^{+}) \quad (1)$$

$$ZnO(e_{cb}^{-}) + Ag \rightarrow ZnO + Ag(e^{-}) \quad (2)$$

$$Ag/ZnO(e^{-}) + O_2 \rightarrow Ag/ZnO + \bullet O_2^{-} \quad (3)$$

$$ZnO(h_{vb}^{+}) + OH^{-} \rightarrow ZnO + \bullet OH \quad (4)$$

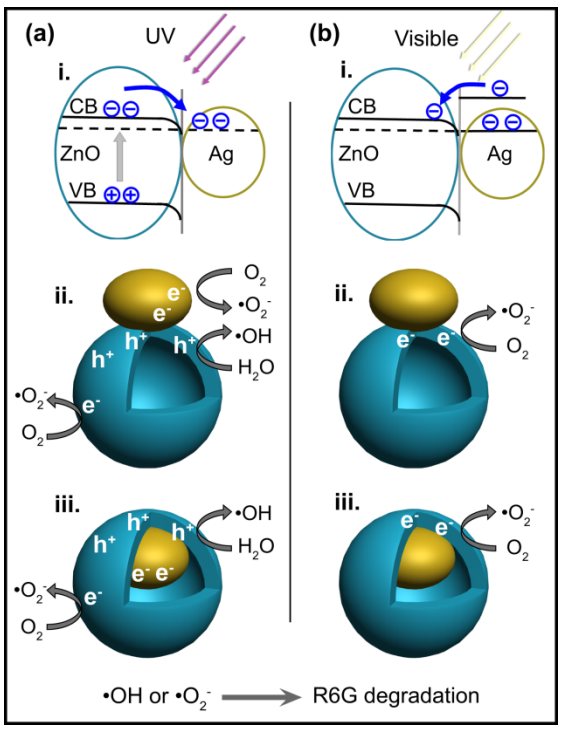

Fig. 6. The energy band gap and photocatalytic mechanisms of asymmetric AOZ and AIZ arrays under (a) UV light and (b) visible light irradiation.

$$\bullet O_2^{-} \text{ or } \bullet OH + R6G \rightarrow \text{degradation of } R6G \quad (5)$$

Since the energy of excited light using the UV lamp with the main wavelength of 365 nm (3.4 eV) is larger than the band gap (~3.3 eV) of ZnO,[36] the electron will be excited to the conduction band (CB) while leaving a vacant state (hole) in the valence band (VB) as in Reaction (1). The photo-generated electron-hole pairs will be easily separated at the Ag/ZnO interface in the Ohmic contact type by transferring the excited electrons in the CB of ZnO to the Ag NPs forced by the built-in electric field. The electrons transferred to Ag NPs and the rest on ZnO HNSs can efficiently react with O_2 molecules adsorbed on the surface of Ag and ZnO to form $\bullet O_2^-$ according to Reaction (2) and (3), as illustrated in Fig. 6a (ii and iii). At the same time, the photo-generated holes located on the surface of ZnO also can react with the H_2O in air to produce another free radical of •OH (Reaction (4)). The generated reactive oxygen species ($\bullet O_2^-$ and •OH) have highly oxidative activity which can effectively degrade the R6G dyes referring to Reaction (5).[41] The reactions discussed above can readily happen both on Ag NPs and ZnO layer in the AOZ structure, where the R6G can be adsorbed. However, in the AIZ hybrid, the ZnO shell layer isolates the R6G molecules from Ag NP inhibiting the reaction contributed by Ag NPs in Reaction (3), and thus reducing the photocatalytic activity of this AIZ structure as shown in Fig. 6a (iii). So, it reasonably explains that a higher photocatalytic activity is presented in the AOZ hybrid rather than the AIZ composite. Of course, the highly localized strong electric-field at the Ag/ZnO interface characterized in above FDTD

simulation results to enhance the light absorption of ZnO HNS is another factor for the improved photocatalytic active on the both asymmetric Ag/ZnO hybrid structures. Besides the electron migration from ZnO to Ag NPs, a little portion of hot electrons would transfer from Ag NPs to ZnO due to the higher order mode LSPRs in Ag NPs at UV irradiation, however, which can be ignored compared with the large number of photo-generated carriers.

While, under the visible light irradiation, the energetic electrons, also called hot electrons, on Ag NPs can be photo-excited to support collective electron oscillations (known as the LSPR effect) as shown in Fig. 6b (i) (Reaction (6)).[42,43] The hot electrons with a sufficient energy can subsequently transfer from the Ag NPs to the conduction band of ZnO to achieve the new thermal equilibrium (Reaction (7)).[41]

$$Ag + h\nu \rightarrow Ag^* \quad (6)$$

$$Ag^* + ZnO \rightarrow Ag + ZnO(e_{cb}^-) \quad (7)$$

$$ZnO(e_{cb}^-) + O_2 \rightarrow ZnO + \bullet O_2^- \quad (8)$$

$$\bullet O_2^- + R6G \rightarrow degradatio\ n\ of\ \ R6G \quad (9)$$

The electrons which accumulate on the surface of ZnO also can be captured by adsorbed O_2 molecules to yield the highly oxidative radical of $\bullet O_2^-$ (Reaction (8)), and then degrade the organic molecules of R6G (Reaction (9)). In this case, the photo-degradation reaction mainly happens on the ZnO layer, which understandably explains the minor differences in degradation rate on AIZ and AOZ arrays with the Ag NP decoration either on or inside the ZnO surface. On the other hand, as shown in Fig. 3a, the differences in LSPR properties for the two samples should also have some contribution to the different degradation rate on AIZ and AOZ arrays. The stronger extinction presented near ~550 nm (the centre emission line of the visible light source) on the AIZ sample would effectively promote the plasmonic assisted photo-degradation reaction. Thus, slightly faster degradation rate was obtained on the AIZ structure than that on AOZ structure as shown in Fig. 5c. By the way, since in visible light irradiation the electron quantities transferring from Ag NPs to ZnO are much less than that from ZnO to Ag NPs under UV illumination, the photo-degradation rate under UV light irradiation is reasonably found to be faster than the corresponding rates in the visible light treatments on both asymmetric hybrids.

3.6. Uniformity for SERS and self-cleaning

In practical applications, uniform and thorough self-cleaning ability on SERS substrates are significantly concerned, which were then characterized by Raman mapping. The Raman mapping image of the AOZ ordered arrays in a large area of 10 μm × 10 μm, as seen in Fig. 7a, is showing the strong and uniform Raman signals as displayed in Fig. 7b, which evidences that the periodic substrate is practically applicable as a SERS substrate. After irradiated by UV and visible light for

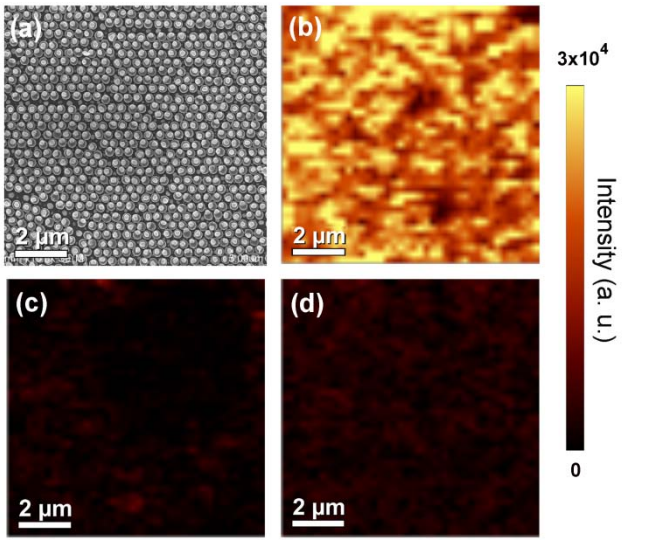

Fig. 7 SEM image of (a) AOZ in an area of 10 μm × 10 μm, and Raman mapping of R6G (10^{-4} M) on AOZ substrates treated by UV light irradiation for (b) 0 min, (c) 90 min, and (d) visible light irradiation for 240 min.

90 and 240 minutes, respectively, the Raman intensity of R6G obviously decreases till invisible, as shown in Fig. 7c-d, demonstrating its good uniformity and efficiency for photo-degradation of R6G molecules. Therefore, an ideal recyclable SERS active substrate with the uniform and thorough self-cleaning functionality can be technically fabricated by configuring the Ag/ZnO asymmetric hybrid structure.

Conclusions

In summary, two asymmetric Ag/ZnO nanocomposite SERS-active substrates with plasmonic assisted UV-visible photo-degradation property were designed and fabricated. The asymmetric dielectric environment around Ag NPs in both structures creates a specific local field enhancement near the contact area of Ag/ZnO, which is not only beneficial for the light absorption in semiconductor, but also in favor of the charge separation and migration between metal and semiconductor. Therefore, besides the highly sensitive SERS performances, self-cleaning functionalities were accomplished on both asymmetric Ag/ZnO composite structures with Ag NPs decorated either on or inside ZnO HNSs' surfaces. The plasmonic assisted photocatalysis is realized with different efficiencies depending on the geometrical configuration of the asymmetric Ag/ZnO composite and energy of the incident light. Electron transfer model based on the band-gap alignment was further proposed to gain insights of the related mechanisms. Given the highly enhanced photocatalytic performance accompanying the reproducible and uniform SERS property, the large area ordered asymmetric metal/semiconductor nanoarrays have been demonstrated to be potentially applicable as recyclable SERS or integrated recyclable sensing chips. Moreover, the concepts and fabrication methods demonstrated in this work can be fundamentally and technically extended to other metal/semiconductor composite systems for broader

researching and applications.

Acknowledgements

This work is financially supported by the MOST of China under the 973 programs (2011CB925600 and 2009CB930704), National Natural Science Foundation of China (61227009, 91321102, 61106118 and 61106008), Science and Technology Project of Fujian Province of China (2013H0046), and Fundamental Research Funds for the Central Universities (2011121026 and 2011121042).

Notes and references

[a] Department of Physics/Pen-Tung Sah Micro-Nano Institute of Science and Technology, Xiamen University, Xiamen, 361005, China. Tel: 86-592-2185962; E-mail: lijing@xmu.edu.cn or jykang@xmu.edu.cn.
[b] Wuhan National Laboratory for Optoelectronics, School of Optical and Electronic Information, Huazhong University of Science and Technology, Wuhan, 430074, China.

† Electronic Supplementary Information (ESI) available: [details of any supplementary information available should be included here]. See DOI: 10.1039/b000000x/

1 R. C. Maher, C. M. Galloway, E. C. Le Ru, L. F. Cohen and P. G. Etchegoin, *Chem. Soc. Rev.*, 2008, **37**, 965.
2 M. L. Zhang, X. Fan, H. W. Zhou, M. W. Shao, J. A. Zapien, N. B. Wong and S. T. Lee, *J. Phys. Chem. C*, 2010, **114**, 1969.
3 D. Graham, D. G. Thompson, W. E. Smith and K. Faulds, *Nat. Nanotechnol.*, 2008, **3**, 548.
4 J. P. Camden, J. A. Dieringer, J. Zhao and R. P. Van Duyne, *Acc. Chem. Res.*, 2008, **41**, 1653.
5 J. N. Anker, W. P. Hall, O. Lyandres, N. C. Shah, J. Zhao and R. P. Van Duyne, *Nat. Mater.*, 2008, **7**, 442.
6 A. M. Michaels, M. Nirmal and L. E. Brus, *J. Am. Chem. Soc.*, 1999, **121**, 9932.
7 Y. H. Feng, Y. Wang, H. Wang, T. Chen, Y. Y. Tay, L. Yao, Q. Y. Yan, S. Z. Li and H. Y. Chen, *Small*, 2012, **8**, 246.
8 X. L. Li, H. L. Hu, D. H. Li, Z. X. Shen, Q. H. Xiong, S. Z. Li and H. J. Fan, *ACS Appl. Mater. Interfaces*, 2012, **4**, 2180.
9 X. X. Zou, R. Silva, X. X. Huang, J. F. Al-Sharab and T. Asefa, *Chem. Commun.*, 2013, **49**, 382.
10 G. Sinha, L. E. Depero and I. Alessandri, *ACS Appl. Mater. Interfaces*, 2011, **3**, 2557.
11 A. Ramakrishnan, S. Neubert, B. Mei, J. Strunk, L. D. Wang, M. Bledowski, M. Muhler and R. Beranek, *Chem. Commun.*, 2012, **48**, 8556.
12 X. H. Li, G. Y. Chen, L. B. Yang, Z. Jin and J. H. Liu, *Adv. Funct. Mater.*, 2010, **20**, 2815.
13 Z. W. Seh, S. H. Liu, M. Low, S. Y. Zhang, Z. L. Liu, A. Mlayah and M. Y. Han, *Adv. Mater.*, 2012, **24**, 2310.
14 A. Mclaren, T. Valdes-Solis, G. Q. Li and S. C. Tsang, *J. Am. Chem. Soc.*, 2009, **131**, 12540.
15 A. B. F. Martinson, J. W. Elam, J. T. Hupp and M. J. Pellin, *Nano Lett.*, 2007, **7**, 2183.
16 J. C. Bernède, Y. Berredjem, L. Cattin and M. Morsli, *Appl. Phys. Lett.*, 2008, **92**, 083304.
17 C. Lizama, J. Freer, J. Baeza and H. D. Mansilla, *Catal. Today,* 2002, **76**, 235.
18 A. A. Khodja, T. Sehili, J. F. Pilichowski and P. Boule, *J. Photochem. Photobiol. A*, 2001, **141**, 231.
19 S. K. Kansal, M. Singh and D. Sud, *J. Hazard. Mater.*, 2007, **141**, 581.
20 P. D. Yang, H. Q. Yan, S. Mao, R. Russo, J. Johnson, R. Saykally, N. Morris, J. Pham, R. R. He and H. J. Choi, *Adv. Funct. Mater.*, 2002, **12**, 323.
21 C. Y. Jiang, X. W. Sun, G. Q. Lo and D. L. Kwong, *Appl. Phys. Lett.*, 2007, **90**, 263501.
22 Y. F. Qiu and S. H. Yang, *Adv. Funct. Mater.*, 2007, **17**, 1345.
23 R. Georgekutty, M. K. Seery and S. C. Pillai, *J. Phys. Chem. C*, 2008, **112**, 13563.
24 M. D. Xiao, R. B. Jiang, F. Wang, C. H. Fang, J. F. Wang and J. C. Yu, *J. Mater. Chem. A*, 2013, **1**, 5790.
25 S. Linic, P. Christopher and D. B. Ingram, *Nat. Mater.*, 2011, **10**, 911.
26 K. Awazu, M. Fujimaki, C. Rockstuhl, J. Tominaga, H. Murakami, Y. Ohki, N. Yoshida and T. Watanabe, *J. Am. Chem. Soc.*, 2008, **130**, 1676.
27 S. C. Warren and E. Thimsen, *Energy Environ. Sci.*, 2012, **5**, 5133.
28 N. Zhang, S. Q. Liu and Y. J. Xu, *Nanoscale*, 2012, **4**, 2227.
29 Y. Li, G. T. Duan, G. Q Liu and W. P. Cai, *Chem. Soc. Rev.*, 2013, **42**, 3614.
30 Y. Li, N. Koshizaki, H. Q. Wang, and Y. Shimizu, *ACS Nano*, 2011, **5**, 9403.
31 .Y. Li, N. Koshizaki, W. P. Cai, *Coordin. Chem. Rev.*, 2011, **255**, 357.
32 J. Yin, Y. S. Zang, C. Yue, Z. M. Wu, S. T. Wu, J. Li and Z. H. Wu, *J. Mater. Chem.*, 2012, **22**, 7902.
33 A. M. Michaels, M. Nirmal and L. E. Brus, *J. Am. Chem. Soc.*, 1999, **121**, 9932.
34 J. F. ;Li, Y. F. Huang, Y. Ding, Z. L. Yang, S. B. Li, X. S. Zhou, F. R. Fan and W. Zhang, *Nature*, 2010, **464**, 392.
35 J. Yin, Y. S. Zang, C. Yue, X. He, J. Li, Z. H. Wu and Y. Y. Fang, *Phys. Chem. Chem. Phys.*, 2013, **15**, 16874.
36 Y. S. Zang, X. He, J. Li, J. Yin, K. Y. Li, C. Yue, Z. M. Wu, S. T. Wu and J. Y. Kang, *Nanoscale*, 2013, **5**, 574.
37 H. Chalabi and M. L. Brongersma, *Nat. Nanotech.*, 2013, **8**, 229.
38 J. Yin, C. Yue, Y. S. Zang, C. H. Chiu, J. C. Li, H. C. Kuo, Z. H. Wu, J. Li, Y. Y. Fang and C. Q. Chen, *Nanoscale*, 2013, **5**, 4436.
39 Z. L. Wang and J. H. Song, *Science*, 2006, **312**, 242.
40 C. Y. Su, L. Liu, M. Y. Zhang, Y. Zhang and C. L. Shao, *Cryst. Eng. Comm.*, 2012, **14**, 3989.
41 T. H. Yang, L. D. Huang, Y. W. Harn, C. C. Lin, J. K. Chang, C. I. Wu and J. M. Wu, *Small*, 2013, **9**, 3169.
42 Y. H. Zheng, L. R. Zheng, Y. Y. Zhan, X. Y. Lin, Q. Zheng and K. M. Wei, *Inorg. Chem.*, 2007, **46**, 6980.
43 H. M. Sung-Suh, J. R. Choi, H. J. Hah, S. M. Koo and Y. C. Bae, *J Photoch. Photobio. A,* 2004, **13**, 37.